



**HAL**  
open science

# Noncovalently Functionalized Monolayer Graphene for Sensitivity Enhancement of Surface Plasmon Resonance Immunosensors

Meenakshi Singh, Michael Holzinger, Maryam Tabrizian, Sinéad Winters,  
Nina C. Berner, Serge Cosnier, Georg S. Duesberg

► **To cite this version:**

Meenakshi Singh, Michael Holzinger, Maryam Tabrizian, Sinéad Winters, Nina C. Berner, et al.. Noncovalently Functionalized Monolayer Graphene for Sensitivity Enhancement of Surface Plasmon Resonance Immunosensors. *Journal of the American Chemical Society*, 2015, 137 (8), pp.2800 - 2803. 10.1021/ja5111512m . hal-01651391

**HAL Id: hal-01651391**

**<https://hal.science/hal-01651391v1>**

Submitted on 16 Dec 2024

**HAL** is a multi-disciplinary open access archive for the deposit and dissemination of scientific research documents, whether they are published or not. The documents may come from teaching and research institutions in France or abroad, or from public or private research centers.

L'archive ouverte pluridisciplinaire **HAL**, est destinée au dépôt et à la diffusion de documents scientifiques de niveau recherche, publiés ou non, émanant des établissements d'enseignement et de recherche français ou étrangers, des laboratoires publics ou privés.



Distributed under a Creative Commons Attribution 4.0 International License

# Monolayer graphene as an efficient double-faced scotch tape for sensitivity enhancement of surface plasmon resonance immunosensors

Meenakshi Singh<sup>††</sup>, Michael Holzinger<sup>†\*</sup>, Maryam Tabrizian<sup>‡</sup>, Sinéad Winters<sup>§</sup>, Nina C. Berner<sup>§</sup>, Serge Cosnier<sup>†\*</sup>, and Georg S. Duesberg<sup>§</sup>

<sup>†</sup>Univ. Grenoble Alpes - CNRS, Département de Chimie Moléculaire, UMR 5250, F-38000 Grenoble, France,

<sup>††</sup>McGill University, Biomax Research Laboratories, Dept. of Biomedical Engineering and Faculty of Dentistry, Montréal, Canada

<sup>‡</sup>School of Chemistry, Centre for Research on Adaptive Nanostructures and Nanodevices (CRANN) and Advanced Materials Bio-Engineering Research Centre (AMBER), Trinity College, Dublin 2, Ireland

## Supporting Information

**ABSTRACT:** A highly efficient surface plasmon resonance (SPR) immunosensor is described using a functionalized single graphene layer on a thin gold film. The aim of this approach was twofold: Firstly, to amplify the SPR signal by growing graphene through chemical vapor deposition and secondly to control the immobilization of biotinylated cholera toxin antigen on copper coordinated nitrilotriacetic acid (NTA) using graphene as an ultrathin double-faced scotch tape. The NTA groups were attached to graphene via pyrene derivatives implying  $\pi$ - $\pi$  interactions. With this setup, an immunosensor for the specific antibody anticholera toxin with a detection limit of 4 pg mL<sup>-1</sup> was obtained. In parallel, NTA polypyrrole films of different thicknesses were electrogenerated on the gold sensing platform where the optimal electropolymerization conditions were determined. For this optimized polypyrrole-NTA setup, the simple presence of a graphene layer between the gold and polymer film led to a clear increase of the SPR signal.

Surface plasmon resonance (SPR) is an established technique for the study of biomolecular interactions and the transduction of biological recognition events in real time without requiring supplemental labelling steps<sup>1</sup>. The principle of this technique is based on light stimulated oscillation of electrons in the conduction band of usually gold films, called resonant surface plasmons. This phenomenon is strongly dependent on the dielectric constant of its environment<sup>2</sup> and represents a great advantage for biosensing applications since a biological receptor-analyte interaction results in a change of the oscillation frequency which can be recorded by measuring the angle change, intensity, refractive index, or phase of the reflected light<sup>1,3</sup>.

Extensive efforts were invested to improve the sensitivity of SPR signals using e.g. gold nanoparticles<sup>4</sup>, quantum dots<sup>5</sup>, or Au/Ag alloy nanocomposites<sup>6</sup>. In terms of targeted immobilization of bioreceptor units on gold surfaces for SPR biosensing, self-assembled (SAM) molecular monolayers<sup>7</sup> or electrogenerated functional polymers<sup>8</sup> are often used. As known, the SPR sensitivity strongly depends on the thickness and dielectric constant of such functional layers on the surface. Therefore, due to a one atom thick sheet of carbon atoms in a hexagonal lattice and the

recent development of its large-scale synthesis and transfer techniques, as well as its functionalization, graphene should be an excellent candidate for SPR signal enhancement<sup>9,10</sup> and label-free monitoring of chemical or biomolecular interactions<sup>11,12</sup>. In addition to its high carrier mobility and zero-band gap characteristics, graphene also exhibits unique and desirable optical properties, such as broadband and tuneable absorptions<sup>13,14</sup>. It has been shown that light transmittance through monolayer graphene is 97.7 %<sup>15</sup>, e.g. a one-atom-thick graphene layer will absorb only 2.3 % of incident light.

Theoretical models have predicted that the incorporation of a single layer of graphene can amplify significantly the optical sensitivity of SPR sensors<sup>16</sup>. The beneficial optical properties of graphene monolayers in the visible light range<sup>17</sup> leads to a change of the propagation constant of surface plasmon polariton (SPP), thus amplifying the change of the refractive index<sup>18</sup>.

Furthermore, biomolecules containing hydrophobic domains or  $\pi$ -systems like DNA strands or proteins tend to adsorb spontaneously on graphene<sup>19</sup>. Graphene can also easily be functionalized<sup>20</sup> and thus be modified for targeted immobilization of bioreceptor units.

Most of the reported graphene based SPR biosensors utilize graphene oxide<sup>21</sup>, reduced graphene oxide<sup>22</sup>, or graphene decorated metal nanoparticles<sup>23,24</sup> as a sensing platform. However, the main limitation of this approach is the lack of homogenous and defect free monolayers on the SPR sensing platform, hindering the exploitation of the benefits of graphene.

Chemical vapour deposition (CVD) growth that can provide large scale monolayers of graphene with low defect densities, is an attractive alternative method to the previously reported SPR substrates<sup>25</sup>. However, so far graphene monolayers for SPR biosensing have been mainly investigated numerically<sup>26</sup> and/or by using non-specific protein adsorption such as bovine serum albumin (BSA) on the SPR chip surface<sup>27</sup>.

This study reports on the beneficial optical properties of a single graphene sheet obtained by CVD for SPR biosensing applications. The ultrathin atomic layer acting as a double-faced scotch tape was used for the controlled immobilization of the receptor unit, antigen cholera toxin by

its modification either with a functional polypyrrole film or pyrene derivatives via  $\pi$ -stacking interactions. Both, the polypyrrole and the pyrene groups contain the anchoring nitrilotriacetic acid (NTA) group for the immobilization of biotin tagged specific receptor, cholera toxin.

The synthesis of graphene and its transfer to gold is described in the Supporting Information (SI). Great care was taken to supply homogeneous graphene, with little defect density and polymer residues<sup>28</sup>, to supply a clean surface for further functionalization. Raman imaging is a very powerful tool to evaluate carbon surfaces. In Figure 1 averaged Raman spectra of single-layer graphene, composed of 10,000 spectra taken over an area of  $40 \times 40 \mu\text{m}$  are shown. On  $\text{SiO}_2$  substrate, D-, G- and 2D peaks appear at  $1350 \text{ cm}^{-1}$ ,  $1583 \text{ cm}^{-1}$ , and  $2680 \text{ cm}^{-1}$ , respectively using  $532 \text{ nm}$  excitation wavelength. The gold substrate spectrum is noisier and has a sloped background due to emission from the metal substrate (Figure 1b)<sup>29,30</sup> The intensity of the graphene peaks is enhanced on  $\text{SiO}_2$  due to interference on the dielectric substrate<sup>31</sup>, which allows a detailed assessment of the graphene quality by Raman imaging shown in Fig S1. While the D band in combination with the D/G band ratio gives insight into the quality of graphene in terms of defects in the graphene's  $\pi$ -system, the 2D band is representative for the number of graphene layers<sup>32</sup>. The Raman spectra in Figure 1 clearly indicate the presence of high quality monolayer graphene due to the almost negligible presence of a D band and the sharp and symmetric 2D band, as well as the high 2D/G peak ratio<sup>33,34</sup>. Further Raman analysis, optical images and XPS spectra showing the continuity and high quality of the graphene are provided in Figure S1 and S3.

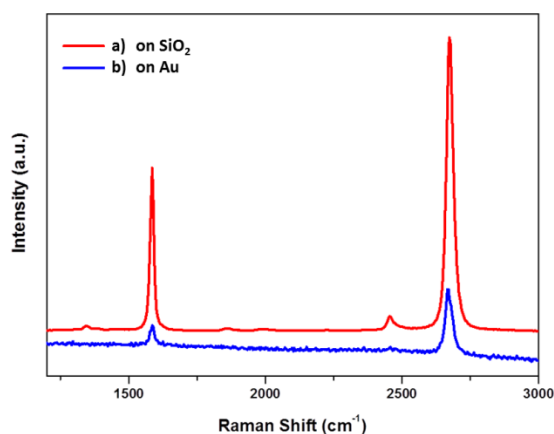


Figure 1. Average Raman spectra of pristine single layer graphene on (a)  $\text{SiO}_2$  and (b) gold substrates.

Effective immobilization of biomolecules on the sensor surface is one of the most challenging steps in the development of high performance biosensors<sup>35</sup>. To secure this requirement, the NTA- $\text{Cu}^{2+}$  / biotin system was used<sup>36</sup>. Furthermore, non-covalent functionalization using  $\pi$ -stacking interactions or electropolymerization was also an important consideration in order to preserve the properties of graphene.

A detailed procedure of the functionalization of the gold surface via electropolymerization of pyrrole-NTA as well as the electrochemical coating and non-covalent attachment of pyrene-NTA can be found in the Supporting Information. Three polymer films of different thicknesses were electrogenerated giving coatings of  $5.66 \text{ nmol.cm}^{-2}$ ;  $16.9 \text{ nmol.cm}^{-2}$  and  $28.3 \text{ nmol.cm}^{-2}$  for the electropolymerization conditions at  $1 \text{ mC.cm}^{-2}$ ,  $3 \text{ mC.cm}^{-2}$ , and  $5 \text{ mC.cm}^{-2}$ , respectively. The resulting

polypyrrole-NTA films were used for the successive attachment of the bioreceptor unit (biotinylated cholera toxin, b-CT) *via* subsequent coordination of copper (II) ions at the NTA chelate and b-CT.

The immunoreaction between the immobilized b-CT and the analyte, anti-cholera toxin from rabbit (anti-CT), was monitored in the angle shift mode in real time. The angle shift is correlated with the changing thickness and optical properties of the sensing layer. The response also depends on the refractive index of the bulk solution. There is a linear relationship between the amount of bound material (analyte) and the SPR angle shift<sup>37</sup>. These angle shifts are in the order of millidegrees ( $\text{m}^\circ$ ) and are used as a response unit to quantify the binding of the analyte to the sensor surface. Control experiments were performed without immobilization of the receptor antigen cholera toxin (table 1) and all experiments were conducted three times to examine the reliability of the assays.

After demonstrating that the thinnest polymer film gives the highest SPR angle change (Figure S2), the conditions for the electropolymerization of such films of  $100 \text{ nm}$  thickness were applied to graphene-modified gold disks. Figure 2 shows the SPR angle change of polypyrrole-NTA/ $\text{Cu}^{2+}$ /b-CT on pure gold films and polypyrrole-NTA/ $\text{Cu}^{2+}$ /b-CT graphene-gold films for  $35 \text{ ng.mL}^{-1}$  and  $4 \text{ ng.mL}^{-1}$  injection of anti-CT. The polypyrrole-NTA/ $\text{Cu}^{2+}$ /b-CT modified graphene-gold slides showed an angle change of  $324 \text{ m}^\circ$  for  $35 \text{ ng.mL}^{-1}$  and  $70 \text{ m}^\circ$  for  $4 \text{ ng.mL}^{-1}$  anti-CT, respectively, which is significantly higher than for the same configuration without the graphene monolayer ( $183 \text{ m}^\circ$  and  $31 \text{ m}^\circ$ , respectively).

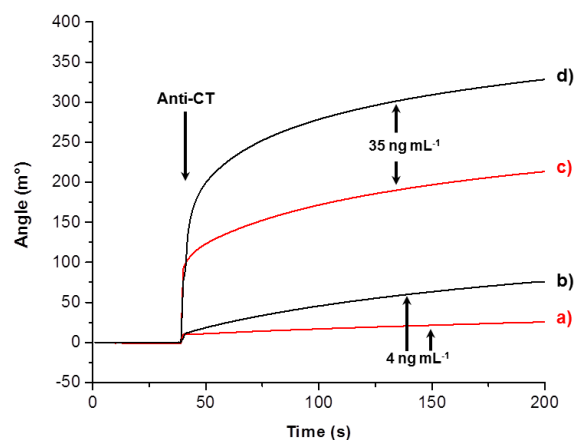


Figure 2. SPR angle shift after anti-CT injection using pure gold (red) and graphene-gold (black) surfaces functionalized with polypyrrole-NTA/ $\text{Cu}^{2+}$ /b-CT at two different anti-CT concentrations (a, b:  $4 \text{ ng.mL}^{-1}$  and c, d:  $35 \text{ ng.mL}^{-1}$ ). The polymer film was formed under controlled potential electrolysis ( $0.95 \text{ V}$ ,  $1 \text{ mC.cm}^{-2}$ ).

For these concentrations of analyte, the simple presence of a graphene monolayer led to an almost two fold increase of the angle shift. Such signal amplification was also observed for the reflectivity mode (table 1). A 9% increase in reflectivity was recorded with graphene-based SPR immnosensor. For pure gold surfaces, the reflectivity change was 7%. A control experiment was performed with gold polypyrrole-NTA/ $\text{Cu}^{2+}$  and graphene-gold polypyrrole-NTA/ $\text{Cu}^{2+}$  in absence of the antigen receptor. For both surface types, a reflectivity change of around 2% with  $35 \text{ ng.mL}^{-1}$  of antibody was recorded for the non-specific binding of the antibody.

One potent method, preserving the unique properties of graphene, is non-covalent functionalization with molecules containing an extended

$\pi$ -system, such as pyrene and its derivatives. In order to keep the sensing layer as thin as possible, pyrene-NTA was  $\pi$ -stacked onto the graphene layer giving a layer of molecular thickness. The successful formation of such a layer was confirmed by XPS measurements, revealing C 1s contributions nearly exclusively from graphene and pyrene-NTA and an estimated thickness of 1.4 nm of the graphene/pyrene-NTA stack, as discussed in the SI. This layer was further stabilized by electropolymerization of the pyrene groups under controlled potential electrolysis. After identical preparation of the immunosensor as for the polypyrrole-NTA setup, the SPR response was measured in angle change and reflectivity mode. An injection of anti-CT at a concentration of 35 ng.mL<sup>-1</sup> led to an angle change of 418 m°. Compared with the best performing polypyrrole-NTA graphene – gold setup (324 m°), the reduced sensing layer thickness improved the SPR immunosensor response by approximately 80 %. This angle shift increase is even more significant when compared with the polypyrrole-NTA setup without graphene (183 m°). Here, the angle change increased 150% (Figure 3). These clear improvements can be attributed not only to the SPR signal amplifying properties of graphene, but also to the possibility to functionalize graphene with SAM techniques using pyrene derivatives.

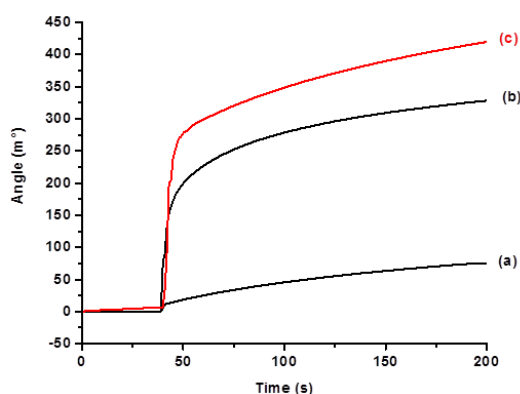


Figure 3: SPR angle change after 35 ng.mL<sup>-1</sup> of anti-CT injection using polypyrrole-NTA/Cu<sup>2+</sup>/b-CT on (a) pure gold and (b) graphene-gold. (c) pyrene-NTA/Cu<sup>2+</sup>/b-CT graphene-gold surface where the pyrene groups were electropolymerized after formation of a monolayer via  $\pi$ -stacking interactions.

Concerning the measurements in reflectivity mode, a 12% increase in reflectivity was recorded with pyrene functionalized graphene-gold SPR immunoensor (table 1).

The increase is again in the two-fold range compared to the most optimized polypyrrole setup without graphene. To determine the limit of detection (LOD), the SPR response was recorded for further dilutions of anti-CT in the angle change mode after 50 s. As shown in Figure 4, a linear range could be determined between 0.004 ng mL<sup>-1</sup> and 4 ng mL<sup>-1</sup> ( $R^2 = 0.9999$ ) with a LOD of 4 pg mL<sup>-1</sup> at a relative standard deviation of 9.2 % of three identical experiments. Such performances are orders of magnitudes higher than comparable electrochemical setups like amperometry<sup>38</sup>, label-free electrochemical impedance spectroscopy<sup>39</sup>, or photoelectrochemical transduction<sup>40</sup>.

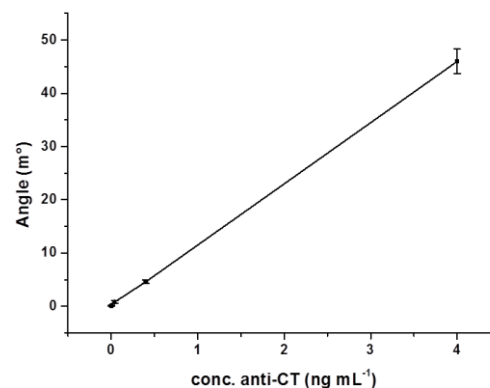


Figure 4: Linear range of the graphene based SPR immunosensor towards anti-CT.

Finally, particular care was taken in characterizing non-specific binding of anti-CT on the functionalized graphene surface. Control experiments were performed under identical conditions by omitting the b-CT immobilization step. In the absence of the antigen receptor unit, a ~2% change in reflectivity and was recorded after injection of 35 ng.mL<sup>-1</sup> of antibody. This is a non-negligible value for non-specific binding of the analyte but represents only 20% of the SPR signal intensity. Other control experiments without receptor unit immobilization using polypyrrole-NTA surfaces or untreated graphene-gold were in the same range. Table 1 represents the data of all SPR responses recorded in angle shift, refractive index, reflectivity mode, as well as captured target biomolecules, including control experiments.

**Table 1 Summary of data obtained on immunosensor performances, including non-specific binding, for modified surfaces**

Sensing surfaces	Angle shift (m°)	Change in reflectivity (%)	Refractive index change (RIU)	Surface density (ng/mm <sup>2</sup> )	Amount (ng)	N° of molecules (10 <sup>11</sup> )
Au-polypyrrole-NTA/Cu <sup>2+</sup> /b-CT (1 mC.cm <sup>2</sup> )	183	7	0.0013	1.50	11.88	5.96
Au- polypyrrole-NTA/Cu <sup>2+</sup> /b-CT (3 mC.cm <sup>2</sup> )	141	3.6	0.0010	1.16	9.17	4.60
Au- polypyrrole-NTA/Cu <sup>2+</sup> /b-CT (5 mC.cm <sup>2</sup> )	102	2	0.0007	0.84	6.66	3.34
Graphene-Au-polypyrrole-NTA/Cu <sup>2+</sup> /b-CT (1 mC.cm <sup>2</sup> )	324	9	0.0023	2.66	21.03	10.55
Graphene-Au-polypyrrole-NTA/Cu <sup>2+</sup> (without antigen)	60	2	0.0004	0.49	3.87	1.94

(1 mC.cm <sup>-2</sup> )						
Graphene-Au-pyrene-NTA/Cu <sup>2+</sup> /b-CT	418	12	0.0029	3.43	27.11	13.6
Graphene-Au-pyrene-NTA/Cu <sup>2+</sup> (without antigen)	53.25	1.2	0.0004	0.43	3.44	1.73
Graphene-Au	71.87	1.5	0.0005	0.58	4.65	2.33

In conclusion, the exceptional optical properties of monolayer graphene in angle change and reflectivity mode were exploited to amplify the SPR signals for cholera immunosensing as a model disease. NTA functional groups were attached to CVD grown graphene via electropolymerization of a polypyrrole film or via  $\pi$ -stacking of pyrene derivatives where this monolayer was further stabilized by electropolymerization. The NTA anchor group served for the controlled immobilization of the biotinylated bioreceptor cholera toxin. The simple presence of a single graphene sheet increased the SPR sensor performances by 80% compared to the graphene-less setup. Furthermore, the best SPR immunosensor was obtained using  $\pi$ -stacking interactions of pyrene-NTA which led to an ultrathin functional layer after electropolymerization.

The clear advantages of the presence of a monolayer graphene and the possibility of ultrathin functional coatings are most likely extensible to other targets for label free SPR immuno- or DNA sensing.

### Supporting Information

Graphene synthesis, transfer and characterization and materials and methods used for the polymer formation layer and experimental details for the determination of the optimal polymer thickness are described in the Supporting Information. This material is available free of charge via the Internet at <http://pubs.acs.org>.

### AUTHOR INFORMATION

#### Corresponding Authors

Correspondence should be addressed to Serge Cosnier ([serge.cosnier@ujf-grenoble.fr](mailto:serge.cosnier@ujf-grenoble.fr)) and Michael Holzinger ([michael.holzinger@ujf-grenoble.fr](mailto:michael.holzinger@ujf-grenoble.fr)).

#### Notes

The authors declare no competing financial interests.

### ACKNOWLEDGMENT

The authors would like to thank the platform 'functionalization of surfaces and transduction' of the scientific structure 'Nanobio' for providing facilities and Arielle Le Pellec for assistance. The authors would also like to thank the French-Canadian Research Found (FCRF) for the Ph.D fellowship for MS and the PHC ULYSSES 2012 PROJET N° 27716UF for travel expenses between France and Ireland. The present work was partially supported by the Labex ARCANE (ANR-11-LABX-0003-01). SW and GSD thank Science Foundation Ireland under SFI-Pica "GREGS" (PI\_10/IN.1/I3030) M. Tabrizian acknowledges NSERC strategic grant contribution to her SPR-based biosensor research.

### References

(1) Wijaya, E.; Lenaerts, C.; Maricot, S.; Hastanin, J.; Habraken, S.; Vilcot, J.-P.; Boukherroub, R.; Szunerits, S. *Current Opinion in Solid State and Materials Science* **2011**, *15*, 208-224.

- (2) Kelly, K. L.; Coronado, E.; Zhao, L. L.; Schatz, G. C. *The Journal of Physical Chemistry B* **2002**, *107*, 668-677.
- (3) Guo, X. *Journal of Biophotonics* **2012**, *5*, 483-501.
- (4) Pedersen, D. B.; Duncan, E. J. S. *Surface Plasmon Resonance Spectroscopy of Gold Nanoparticle-Coated Substrates*, Defence R&D Canada, 2005.
- (5) Malic, L.; Sandros, M. G.; Tabrizian, M. *Analytical Chemistry* **2011**, *83*, 5222-5229.
- (6) Wang, J.; Song, D.; Wang, L.; Zhang, H.; Zhang, H.; Sun, Y. *Sensors and Actuators B: Chemical* **2011**, *157*, 547-553.
- (7) Chaki, N. K.; Vijayamohan, K. *Biosensors and Bioelectronics* **2002**, *17*, 1-12.
- (8) Cosnier, S.; Holzinger, M. *Chem. Soc. Rev.* **2011**, *40*, 2146-2156.
- (9) Geim, A. K. *Science* **2009**, *324*, 1530-1534.
- (10) Geim, A. K.; Novoselov, K. S. *Nat Mater* **2007**, *6*, 183-191.
- (11) Wang, Y.; Li, Z.; Wang, J.; Li, J.; Lin, Y. *Trends Biotechnology* **2011**, *29*, 205-212.
- (12) Salavagione, H. J.; Diez-Pascual, A. M.; Lazaro, E.; Vera, S.; Gomez-Fatou, M. A. *Journal of Materials Chemistry A* **2014**, *2*, 14289-14328.
- (13) Bonaccorso, F.; Sun, Z.; Hasan, T.; Ferrari, A. C. *Nat Photon* **2010**, *4*, 611-622.
- (14) Bao, Q.; Loh, K. P. *ACS Nano* **2012**, *6*, 3677-3694.
- (15) Nair, R. R.; Blake, P.; Grigorenko, A. N.; Novoselov, K. S.; Booth, T. J.; Stauber, T.; Peres, N. M. R.; Geim, A. K. *Science* **2008**, *320*, 1308-1308.
- (16) Wu, L.; Chu, H. S.; Koh, W. S.; Li, E. P. *Optics Express* **2010**, *18*, 14395-14400.
- (17) Bruna, M.; Borini, S. *Applied Physics Letters* **2009**, *94*, 031901.
- (18) Jacek, G.; Dawn, T. H. T. *Nanotechnology* **2013**, *24*, 185202.
- (19) Song, B.; Li, D.; Qi, W.; Elstner, M.; Fan, C.; Fang, H. *ChemPhysChem* **2010**, *11*, 585-589.
- (20) Georgakilas, V.; Otyepka, M.; Bourlinos, A. B.; Chandra, V.; Kim, N.; Kemp, K. C.; Hobza, P.; Zboril, R.; Kim, K. S. *Chemical Reviews* **2012**, *112*, 6156-6214.
- (21) Chiu, N.-F.; Huang, T.-Y.; Lai, H.-C.; Liu, K.-C. *Nanoscale Research Letters* **2014**, *9*, 1-7.
- (22) Wang, L.; Zhu, C.; Han, L.; Jin, L.; Zhou, M.; Dong, S. *Chemical Communications* **2011**, *47*, 7794-7796.
- (23) Zhang, H.; Song, D.; Gao, S.; Zhang, J.; Zhang, H.; Sun, Y. *Sensors and Actuators B: Chemical* **2013**, *188*, 548-554.
- (24) Zhang, J.; Sun, Y.; Xu, B.; Zhang, H.; Gao, Y.; Zhang, H.; Song, D. *Biosensors and Bioelectronics* **2013**, *45*, 230-236.
- (25) Wirtz, C.; Lee, K.; Hallam, T.; Duesberg, G. S. *Chemical Physics Letters* **2014**, *595-596*, 192-196.
- (26) Choi, S. H.; Kim, Y. L.; Byun, K. M. *Optics Express* **2011**, *19*, 458-466.
- (27) Szunerits, S.; Maalouli, N.; Wijaya, E.; Vilcot, J.-P.; Boukherroub, R. *Analytical and Bioanalytical Chemistry* **2013**, *405*, 1435-1443.
- (28) Hallam, T.; Berner, N. C.; Yim, C.; Duesberg, G. S. *Advanced Materials Interfaces* **2014**, *1*, n/a-n/a.
- (29) Xu, W.; Xiao, J.; Chen, Y.; Chen, Y.; Ling, X.; Zhang, J. *Advanced Materials* **2013**, *25*, 928-933.
- (30) Kim, N.; Oh, M. K.; Park, S.; Kim, S. K.; Hong, B. H. *Bulletin of the Korean Chemical Society* **2010**, *31*, 999 - 1003.
- (31) Wang, Y. Y.; Ni, Z. H.; Shen, Z. X.; Wang, H. M.; Wu, Y. H. *Applied Physics Letters* **2008**, *92*, -.
- (32) Ferrari, A. C.; Basko, D. M. *Nat Nano* **2013**, *8*, 235-246.

- (33) Wink, T.; J. van Zuilen, S.; Bult, A.; P. van Bennekom, W. *Analyst* **1997**, *122*, 43R-50R.
- (34) Ferrari, A. C.; Meyer, J. C.; Scardaci, V.; Casiraghi, C.; Lazzeri, M.; Mauri, F.; Piscanec, S.; Jiang, D.; Novoselov, K. S.; Roth, S.; Geim, A. K. *Physical Review Letters* **2006**, *97*, 187401.
- (35) Sicard, C.; Brennan, J. D. *MRS Bulletin* **2013**, *38*, 331-334.
- (36) Baur, J.; Holzinger, M.; Gondran, C.; Cosnier, S. *Electrochem. Comm.* **2010**, *12*, 1287-1290.
- (37) Stenberg, E.; Persson, B.; Roos, H.; Urbaniczky, C. *Journal of Colloid and Interface Science* **1991**, *143*, 513-526.
- (38) Ionescu, R. E.; Gondran, C.; Cosnier, S.; Gheber, L. A.; Marks, R. S. *Talanta* **2005**, *66*, 15-20.
- (39) Haddour, N.; Chauvin, J.; Gondran, C.; Cosnier, S. *J. Am. Chem. Soc.* **2006**, *128*, 9693-9698.
- (40) Yao, W.; Le Goff, A.; Spinelli, N.; Holzinger, M.; Diao, G.-W.; Shan, D.; Defrancq, E.; Cosnier, S. *Biosensors and Bioelectronics* **2013**, *42*, 556-562.

# Table of Contents artwork

---

